



Faculty Scholarship

4-2021

Quantification of the Effects Of Hydrophobicity and Mass Loading on the Effective Coverage of Surface-Immobilized Elastin-like Peptides

Zihang Su
Case Western Reserve University

Julie N. Renner
Case Western Reserve University, julie.renner@case.edu

Author(s) ORCID Identifier:

 Zihang Su

 Julie N. Renner

Follow this and additional works at: <https://commons.case.edu/facultyworks>

Recommended Citation

Su, Zihang and Renner, Julie N., "Quantification of the Effects Of Hydrophobicity and Mass Loading on the Effective Coverage of Surface-Immobilized Elastin-like Peptides" (2021). *Faculty Scholarship*. 55.
<https://commons.case.edu/facultyworks/55>

This Article is brought to you for free and open access by Scholarly Commons @ Case Western Reserve University. It has been accepted for inclusion in Faculty Scholarship by an authorized administrator of Scholarly Commons @ Case Western Reserve University. For more information, please contact digitalcommons@case.edu.

1 Quantification of the Effects of Hydrophobicity and
2 Mass Loading on the Effective Coverage of Surface-
3 Immobilized Elastin-like Peptides

4 *Zihang Su,^a ChulOong Kim,^b Julie N. Renner^{a,*}*

5 a. Department of Chemical and Biomolecular Engineering, Case Western Reserve University,
6 Cleveland, Ohio 44106, United States

7 b. Department of Chemical and Biological Engineering, Colorado School of Mines, Golden,
8 Colorado 80401, United States

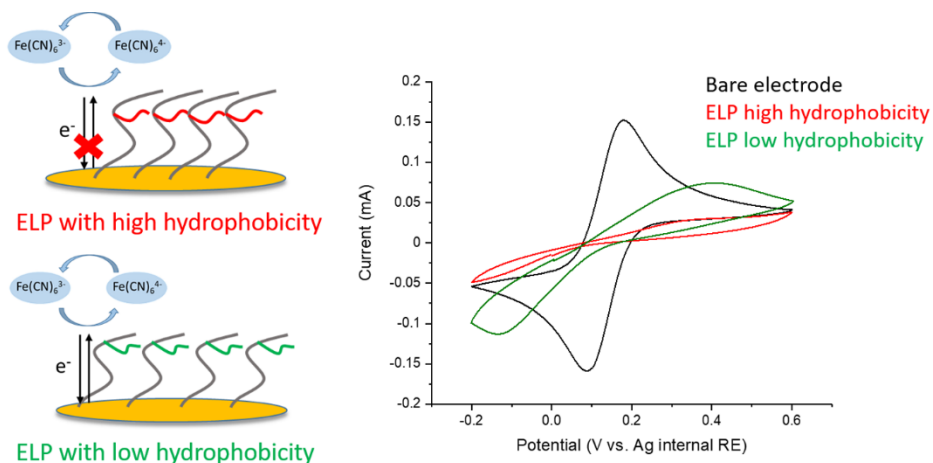
9 *Corresponding author: jxr484@case.edu

10 **Abstract**

11 Elastin-like peptides (ELPs) immobilized to solid surfaces have recently gained attention for use
12 in electrochemical applications in sensing as well as bioenabled electrode assembly. Key to the
13 success of these applications is understanding how ELPs impact the access and electron transfer
14 of reacting species to the solid surface (effective surface coverage). In this study, short ELPs with
15 varying hydrophobicity and sequence length were designed for gold attachment, and the effect on
16 the ability of a redox probe to access a gold surface was characterized by cyclic voltammetry. A
17 quantitative model describing the relationship between ELP effective surface coverage as a
18 function of mean hydrophobicity and mass loading was elucidated based on the results, showing

19 the ability to precisely control surface properties by tuning the ELP sequence. This model will be
20 useful for the design of surface-bound ELP sequences that exhibit desired effective surface
21 coverage for electrochemical as well as biomaterial applications.

22 Graphical abstract



23 Surface properties are controlled by tuning elastin-like peptide sequences

24 Keywords

25 Elastin-like polypeptides, electrode modification, cyclic voltammetry, biotechnology

26 1. Introduction

27 Recently, protein and polypeptide engineering have emerged as promising tools for
28 electrochemical applications. Taking advantage of the ability to precisely define sequences and
29 achieve multiple specific functions, protein and polypeptide-containing thin film electrode
30 modifications have already been applied to biosensing, enzyme-based electrode design, and
31 biomedical device manufacturing [1–3].

32 Elastin is a particularly attractive polypeptide platform for electrochemical applications.
33 Engineered elastin-like polypeptide sequences (ELPs) are derived from the hydrophobic
34 domains of tropoelastin, with a repetitive motif consisting of Val-Pro-Gly-Xaa-Gly, where
35 X is a guest residue that can be substituted by any amino acid except proline [4]. ELPs are
36 well-known as stimuli-responsive biopolymers, exhibiting reversible thermal-dependent
37 lower solution critical temperature (LCST) behavior in aqueous solutions, where they are
38 soluble below the transition temperature and insoluble above it. This transition temperature
39 (T_i) is dependent on the environmental conditions [5,6] as well as peptide concentration,
40 chain length [7], and hydrophobicity [8]. With these unique sequence-defined
41 characteristics, including stimulus-responsive and self-assembly behavior, ELPs have been
42 designed for variety of applications, such as: protein purification, drug delivery, and tissue
43 engineering [9]. The transition behavior of ELPs is also maintained in immobilized
44 assemblies, leading to surface-bound “smart” applications [10].

45 Label-free electrochemical sensing platforms based on ELP transducers assembled on gold
46 surfaces have recently been explored, where elastin in the insoluble state blocks electron
47 transfer between a redox probe, specifically the common $\text{Fe}(\text{CN})_6^{3-/4-}$ redox couple, and
48 the gold electrode surface [11]. When the immobilized elastin is in the soluble state, the
49 redox probe can access the electrode surface and electron transfer happens more readily. In
50 essence, the current changes observed are indicative how exposed the gold surface is to the
51 electrolyte when modified with molecular layers [12]. However, the impact of changing the
52 assembled ELP guest residue content and mass loading on surface exposure, as measured
53 via electron transfer performance between a redox probe and the gold electrode, is largely
54 unexplored. The sensitivity of elastin-based electrochemical sensing platforms depends on

55 the differences in surface exposure, which may vary depending on the chosen ELP
56 sequence. In addition, the application of ELPs has expanded to bioenabled electrode
57 assembly, where surface access and chemical versatility is desired [13–17]. There has also
58 been a particular recent interest in exploiting the responsive behavior of short elastin
59 polypeptides on functionalized gold nanoparticles [18], which is useful in other non-
60 electrochemical areas including drug delivery [19], imaging [20], and as active plasmonic
61 waveguides [21]. Surface exposure is also important in these applications, as exposed
62 substrates may be prone to biofouling [22].

63 In this study, we hypothesize that surface access (or effective surface coverage), as
64 measured via electron transfer between a redox probe and the gold electrode, can be
65 controlled by modifying the guest residue hydrophobicity and mass loading of assembled
66 engineered short ELPs. Herein, we utilized cyclic voltammetry (CV) to investigate the
67 effective surface coverage of different ELPs when assembled on gold electrodes with
68 varying guest residues and length. A quartz crystal microbalance with dissipation (QCM-
69 D) was utilized to estimate the mass loading and observe the layer formation process. The
70 results show that effective surface coverage can be precisely and predictably tuned using
71 assembled ELPs. The proposed model for effective surface coverage will serve as guidance
72 for future ELP-based electrochemical sensing platforms and electrode design.

73

74

75

76 **2. Materials and methods**

77 **2.1 Materials**

78 Detailed materials information is provided in the Supplementary Data.

79 **2.2 Peptide design**

80 Peptide sequences utilized in this study consisted of an elastin-like motif, (VPGXG)_n, where n =
81 number of pentapeptide repeats. The N-terminus was modified with cysteine (C) for all peptides.
82 The ends of the peptides were acylated and amidated. All sequences are shown in Table S1. All
83 peptides were purchased from GenScript at purities above 95%.

84 **2.3 Electrode preparation**

85 Screen printed electrodes (Metrohm DropSens, DRP-220BT, L33 × W10 × H0.5 mm) with a gold
86 working electrode (4 mm diameter), silver reference electrode, and platinum counter electrode
87 were used in this study. Before electrode functionalization, all SPEs were prepared by cleaning in
88 0.5 M H₂SO₄ solution (60 μL to fully cover the SPE electrodes), performing cyclic voltammetry
89 scans from -0.2 V to 1.3 V (versus internal silver reference electrode) at the scan rate of 100 mV
90 s⁻¹, with 9 scans accumulations [23]. After cleaning, SPEs were rinsed with deionized (DI) water
91 and dried with N₂. All SPEs were used once per test in this study, and not reused.

92 **2.4 Peptide incubation**

93 All peptides were prepared at 10 μg/mL in 0.01 M phosphate buffered saline (PBS, pH 7.4). For
94 experiments on screen-printed electrodes, 60 μL of the peptide solution was deposited on the SPE
95 electrode surface. The same amount of PBS solution (60 μL) was added for the bare electrode

96 experiments. To ensure the electrode surface was maximally saturated with peptide adsorption, all
97 SPE samples were incubated for overnight at 4°C. Prior to electrochemical characterization,
98 electrodes were gently rinsed with PBS solution and dried with N₂ gas. All peptide solutions were
99 prepared freshly prior to experiments. In buffer concentration experiments, all solutions were made
100 in 0.1 M PBS (pH=7.4) unless otherwise stated.

101 **2.5 Cyclic voltammetry**

102 All electrochemical experiments were performed on SPEs that connected to a Metrohm Autolab
103 potentiostat (controlled by Nova 2.1 software). The redox buffer contained equimolar amounts of
104 4 mM K₃Fe(CN)₆ and 4 mM K₄Fe(CN)₆ in 0.01 M PBS (pH 7.4) with 0.1 M KCl. Cyclic
105 voltammetry (CV) measurements on SPEs were conducted at room temperature, at a range of -0.2
106 V to 0.6 V and a scan rate of 100 mV s⁻¹ without any preconditional potential or accumulation time.
107 For each sample, 60 μL redox solution was used to fully cover the SPE electrodes, and five scans
108 were collected. In forward of CV scans, ferrocyanide is oxidized to ferricyanide, and in reverse
109 scans, ferricyanide is reduced to ferrocyanide. Experiments with varying scan rate were collected
110 using equimolar amounts of 5 mM K₃Fe(CN)₆ and 5 mM K₄Fe(CN)₆ in 0.01 M PBS (pH 7.4) with
111 0.1 M KCl at a range of 10-100 mV s⁻¹. Redox probe concentration experiments were collected
112 with equimolar solutions from 0 to 100 mM in 0.01 M PBS with 0.1M KCl solution at 50 mV s⁻¹.

113 **2.6 Quartz crystal microbalance with dissipation**

114 A quartz crystal microbalance with dissipation (QCM-D, QSense Explorer, controlled by QSoft
115 software, Biolin Scientific) was used to investigate the peptide adsorption behavior and the relative
116 mass loading of each peptide on gold surfaces. Frequency shifts and dissipation changes were

117 monitored simultaneously versus time. The details of these experiments can be found in our
118 previous work [15,16], and in the Supplementary Data.

119 **2.7 Circular dichroism**

120 Circular dichroism (CD) spectroscopy was utilized to analyze the secondary structure of triple-
121 repeat elastin-like peptides. Procedures can be found in our previous work [16], with details in the
122 Supplementary Data.

123 **2.8 Atomic force microscopy**

124 Atomic force microscopy (AFM) was used to analyze the topography of surface-immobilized
125 triple-repeat elastin-like peptides VKV and KVK. Procedures can be found in our previous
126 works[15,16], with details in the Supplementary Data.

127 **2.9 Statistical analysis**

128 Data are represented as the mean \pm the standard deviation. Analysis of variance (ANOVA) was
129 performed using Minitab to determine if a factor had a significant effect. Statistical groupings were
130 determined by Tukey's *post hoc* test. Simple linear regression of average values was performed
131 using Minitab. Best fit lines are obtained using the method of least squares. All statistical tests
132 used $\alpha = 0.05$. For results in the main text, $n = 3$ except in the case of single-repeated peptide where
133 $X = E$ ($n = 5$) and triple-repeated peptide where $X = K_3$ ($n=4$).

134

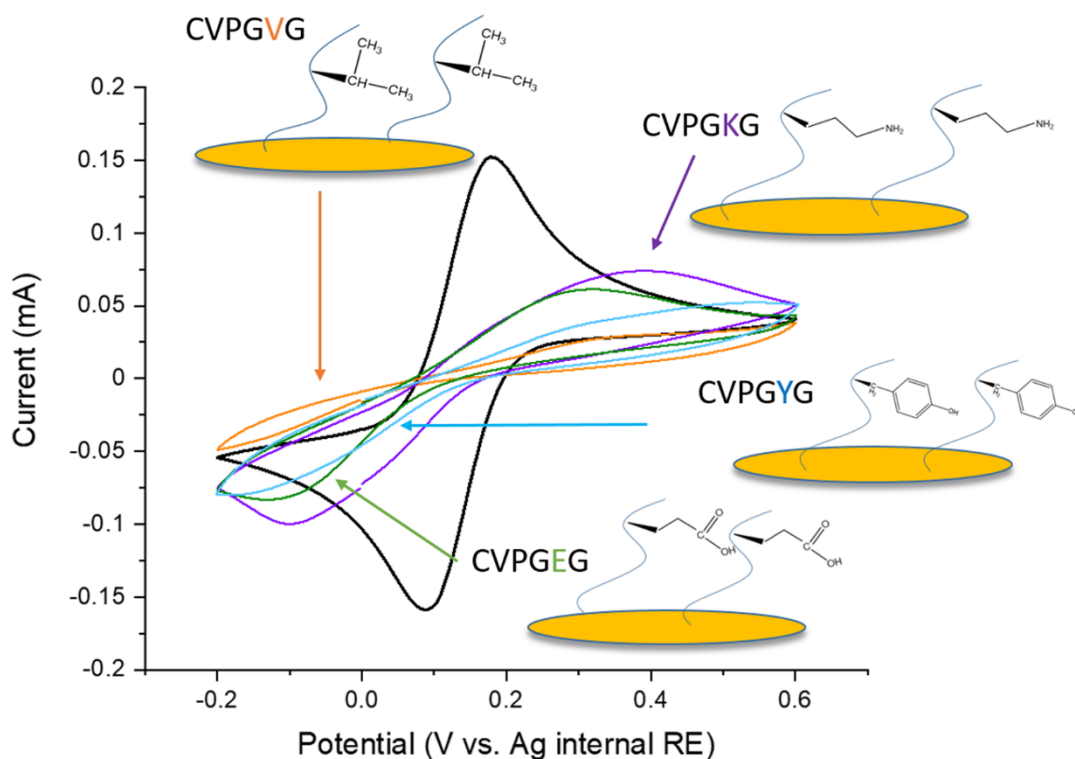
135

136

137 **3. Results**

138 **3.1 The influence of gold-immobilized single-repeat ELP guest residue on**
139 **Fe(CN)₆^{3-/4-} electron transfer**

140 Cyclic voltammetry (CV) was performed in the presence of a Fe(CN)₆^{3-/4-} redox probe on
141 gold electrodes with assembled ELPs. To investigate the effect of guest residue
142 hydrophobicity, single-repeat elastin peptides with different guest residues were designed
143 with the sequence Ac-CVPGXG-NH₂, featuring an N-terminal cysteine (C) for rapid
144 immobilization to the gold surface via a thiol bond. Table S1 contains all sequences
145 explored in this study. All peptides were acetylated and amidated to ensure any charge
146 effects were imparted only by the guest residues. Lysine (K) and glutamic acid (E), served
147 respectively as positively and negatively charged guest residues. Valine (V) and tyrosine
148 (Y) were selected as neutral guest residues of varying hydrophobicity. The single-repeat
149 peptides were assembled on prepared screen printed electrodes (SPEs) and exposed to the
150 redox solution. Each CV experiment consisted of five scans. Stable data indicated the
151 assembled elastin did not change significantly during the scanning period (Figure S1).
152 Representative CVs are shown in Figure 1.



153

154 **Figure 1.** Cyclic voltammograms obtained on ELP-modified SPEs with varying ELP guest
 155 residue hydrophobicity demonstrate controlled electron transfer of a label-free redox probe.
 156 Results were collected in 0.01 M PBS with 4 mM $\text{Fe}(\text{CN})_6^{3-/4-}$ redox couple and 0.1 M KCl,
 157 from -0.2 V to 0.6 V (vs. silver internal reference electrode) with a 0.1 V/s scan rate.
 158 Representative data are shown, and include bare gold SPE electrode (black), V modified
 159 electrode (orange), K modified electrode (purple), E modified electrode (green), and Y
 160 modified electrode (blue).

161

162 On bare gold electrodes, as shown in Figure 1 (black line), a pair of redox peaks was
 163 observed, with a peak-to-peak separation of ~60 mV which is expected for diffusion-

164 controlled, reversible redox reactions. In contrast, CVs taken on peptide-modified
165 electrodes either had no discernible peaks, or had increased peak-to-peak separations,
166 which is indicative of a quasi-reversible redox reaction. Plots of peak current versus the
167 square root of scan rate for selected peptides in this study (Figure S2) confirm the quasi-
168 reversible nature, with slight deviations from perfect linearity observed. In addition, the
169 peak currents observed on peptide-modified electrodes were lower compared to peak
170 currents observed on bare electrode. The results indicated that all ELPs were successfully
171 immobilized on electrode surface, and different peptide layers were reducing the available
172 electrode surface area or hindering the ability of electron transfer from the redox probe in
173 solution to the underlying electrode.

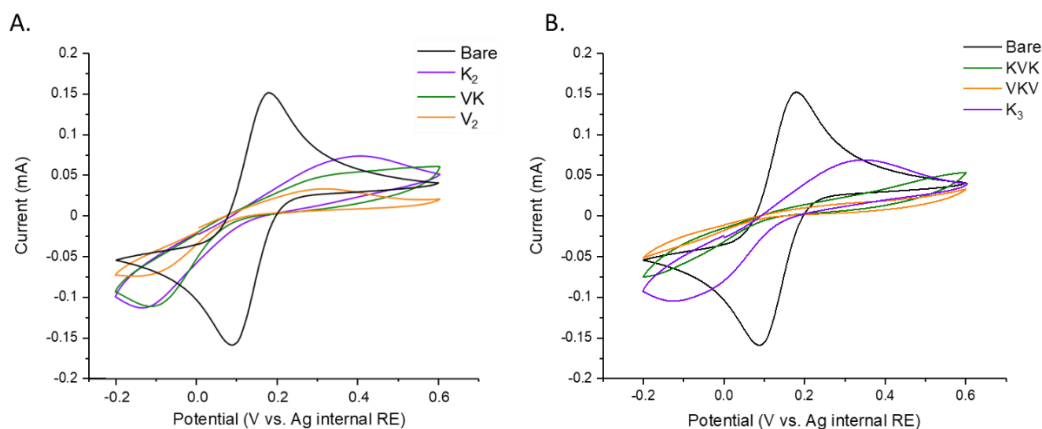
174 To quantify the extent to which the peptides block electron transfer, the total charge passed
175 on the second CV scan of each peptide sample was normalized to the bare gold electrode
176 sample. Thus, to compare samples we define effective surface coverage, f_e , as:

177 Equation 1: $f_e = 1 - \frac{\text{total charge for sample } (C_i)}{\text{total charge for bare gold } (C_0)}$

178 Using this definition, we discovered f_e was guest residue dependent, being 0.24 ± 0.03 , 0.37
179 ± 0.12 , 0.43 ± 0.11 , 0.57 ± 0.02 for guest residue $X = K, E, Y$ and V , respectively. We
180 observed that in general f_e was positively related to hydrophobicity, with immobilized
181 peptides containing guest residue $X = V, Y$ and E in one statistical grouping, and $X = Y,$
182 K, E being in another statistical grouping (see Table S2 for ANOVA and *post hoc* testing
183 results), indicating that hydrophobicity of the guest residue has a significant impact on
184 electron transfer.

185 **3.2 The influence of gold-immobilized double- and triple-repeat ELP guest residue**
186 **on $\text{Fe}(\text{CN})_6^{3-/4-}$ electron transfer**

187 To further investigate the effects of ELP guest residue hydrophobicity and length in
188 controlling f_e , double- and triple-repeat ELPs were designed with varying ratios of
189 positively charged guest residue (K) and neutral hydrophobic guest residue (V) (Table S1
190 contains exact peptide sequences). Briefly, three double-repeat peptides were designed
191 having the general form of $\text{Ac-CVPGX}_1\text{GVPGX}_2\text{G-NH}_2$, with guest residues occurring in
192 the order $X_1X_2 = \text{K}_2, \text{VK}$ and V_2 . Three triple-repeat peptides were designed with the
193 general form of $\text{Ac-CVPGX}_1\text{GVPGX}_2\text{GVPGX}_3\text{G-NH}_2$, with guest residues occurring in
194 the order $X_1X_2X_3 = \text{K}_3, \text{KVK}$ and VKV . Figure 2 shows the representative CV scans on
195 double- and triple- repeat peptide functionalized electrodes as well as a bare gold electrode
196 for comparison.



197
198 **Figure 2.** Cyclic voltammograms demonstrate that the average guest residue hydrophobicity of
199 double- and triple-repeat elastin peptides assembled on gold impact the electron transfer of a label-
200 free redox probe. Results were collected in 0.01 M PBS with 4 mM $\text{Fe}(\text{CN})_6^{3-/4-}$ redox couple and

201 0.1 M KCl, from -0.2 V to 0.6 V (vs. silver internal reference electrode) with a 0.1 V/s scan rate.
202 Representative cyclic voltammograms are shown for (A) bare electrode (black), K₂ (purple), VK
203 (green), and V₂ (orange); (B) bare electrode (black), K₃ (purple), KVK (green) and VKV (orange).

204
205 The CVs obtained on electrodes functionalized with double- and triple-repeat ELPs
206 exhibited a similar trend shown in Figure 1, where it was observed that as the fraction of V
207 increases, the average hydrophobicity increases, and f_e increases, coinciding with an
208 increase in peak-to-peak separation and decrease in peak current. For electrodes
209 functionalized with double-repeat ELPs K₂, VK, and V₂, f_e was 0.23 ± 0.06 , 0.43 ± 0.10 ,
210 and 0.57 ± 0.03 , respectively. On triple-repeat ELP-modified electrodes with K₃, KVK and
211 VKV, f_e was 0.32 ± 0.03 , 0.55 ± 0.09 , and 0.77 ± 0.04 , respectively. ANOVA and *post hoc*
212 analysis (Tables S3 and S4) indicated that the average hydrophobicity of the guest residues
213 had a significant impact on electron transfer for double- and triple repeat peptide samples.

214

215 **3.3 A quantitative model for effective surface coverage**

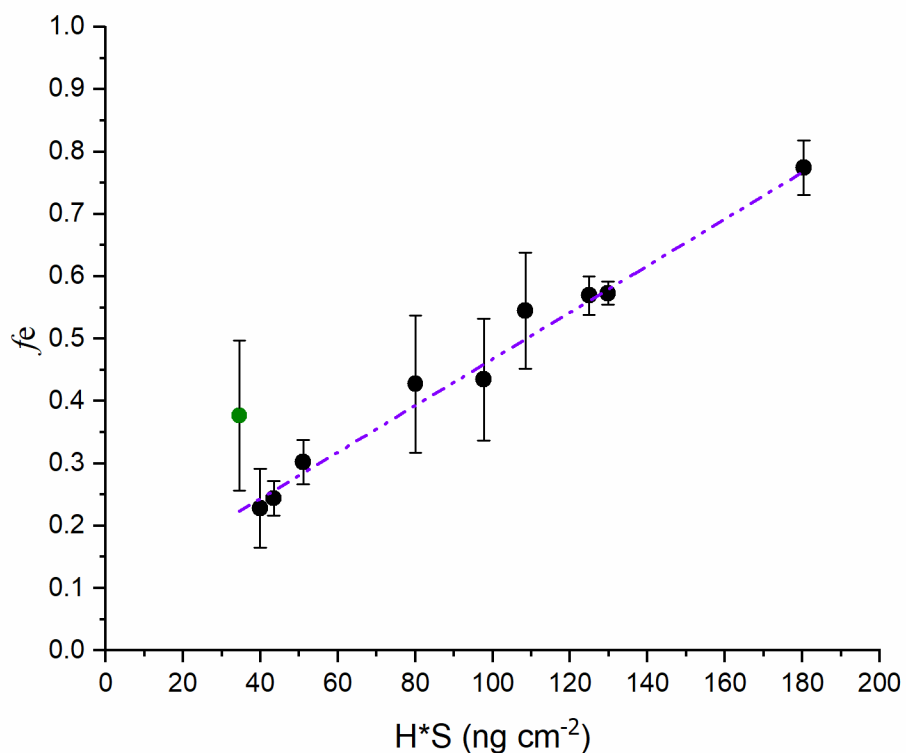
216 To compare the relative mass loading on gold electrodes of different ELPs, hydrated mass
217 loading of ELPs were estimated using a quartz crystal microbalance with dissipation
218 (QCM-D). Table S5 shows estimated relative hydrated mass loadings for all peptides in
219 this study, and Figure S3 shows representative QCM-D runs of triple-repeat ELPs.

220 Given that relative mass loading and hydrophobicity were hypothesized to significantly
221 affect the f_e , we proposed the following model:

222 Equation 2: $f_e = k_e S (H) + f_{e,min}$

223 Where k_e is a parameter to describe the dependence of f_e on hydrophobicity and
224 pentapeptide loading ($\text{cm}^2 \text{ng}^{-1}$), S is the mass loading of elastin per unit area (ng cm^{-2}), and
225 $f_{e,min}$ is the minimal amount of coverage for a monolayer of elastin. H is the relative
226 hydrophobicity normalized to valine such that H is the average hydrophobicity compatibility
227 index of the guest residues divided by the hydrophobicity compatibility index of valine[24].
228 Calculation examples are provided in Table S6.

229 Based on Equation 2, a plot of f_e versus $H*S$ will yield a straight line, where the slope is
230 equal to k_e and the intercept represents $f_{e,min}$. Figure 3 shows f_e values calculated from data
231 represented in Figure 1 and 2 plotted as a function of $H*S$. Linear regression was performed
232 on average values and the linear relationship between f_e and $H*S$ was statistically
233 significant (see Figure S4, and Table S7 for regression results).



234

235 **Figure 3.** Effective coverage, f_e , is linearly related to hydrophobicity compatibility with valine (H)
 236 multiplied by the mass loading (S) of ELPs immobilized on gold. Each data point represents the
 237 average \pm the standard deviation for at least $n = 3$ independent trials. A simple linear regression
 238 was performed using Minitab, and the purple line represents the best fit line. Results from the
 239 linear regression can be found in the Supplementary Data. The data point in green represents an
 240 outlier that is not included in the linear regression for the final model.

241

242 Conditions such as scan rate, redox probe concentration and PBS concentration were varied
 243 to identify impact on the model. Experiments conducted at different scan rates are provided
 244 in Supplementary Data Figure S5 and S6. Based on the results, scan rate needs to be sufficiently

245 high for the model to be valid. Redox probe concentration was varied, and data collected on VKV
246 peptide-modified SPEs (Figure S7). When the redox concentration $> 1\text{mM}$, peak current is 100X
247 greater or more compared to the control of 0 mM redox probe. Thus, the concentration was
248 sufficiently high in experiments used to develop the model. In addition, Figure S7B shows that
249 there is a linear relationship between peak current and concentration, indicating that the redox
250 probe concentration does not significantly change the properties of the assembled peptide layer.
251 The effect of higher PBS concentrations on the model is shown in Figure S8, where 10X PBS
252 results in a linear relationship between fe and H^*S , but the slope is lower (~ 0.0015). This indicates
253 that the model is valid at higher salt concentrations and sufficiently high scan rates, but the slope
254 may be dependent on ionic strength.

255

256 An alternative model based on ELP length instead of mass loading is provided in the
257 Supplementary Data (Figure S9). In the alternative model, fe is a linear function of H/L , where
258 each length of peptide has its own distinct slope and L = the number of elastin repeats. As the
259 peptide length increases, the slope increases, indicating the dependence of fe on H/L becomes
260 stronger such that a small change in hydrophobicity for a long peptide will have a greater impact
261 on fe . Previous studies have shown that more intermolecular aggregations and hydrophobic
262 collapse happens when ELP length increases.[5,25] Overall, the alternative model based on length
263 provides additional evidence that fe may be impacted by the number of hydrophobic interactions
264 in an ELP layer, indicated by the model based on mass loading in Figure 3 (see Discussion section
265 for more insight into this result).

266

267 3.4 The effect of guest residue charge on peptide assembly

268 The data gathered with the single repeat peptide where X = a negatively charged glutamic
269 acid (E) was higher than expected (shown in green in Figure 3). Figure S3A shows that the
270 data point lies outside of the 95% confidence interval for the linear relationship. Without
271 the outlier, linear regression results in $k_e = 0.0038 \pm 0.0004 \text{ cm}^2 \text{ ng}^{-1}$ and $f_{e,min} = 0.093 \pm$
272 0.046 (95% confidence intervals). To investigate if the electrostatic effect during peptide
273 assembly, we exposed E and K peptides to acidic and basic environments, respectively, to
274 neutralize the guest residues. CV experiments were performed after the assembly in
275 neutralized conditions to quantify the impact on f_e . As demonstrated in Figure S10, peptides
276 assembled under neutral conditions had the same CV results as when they were assembled
277 in their charged states. This result suggests the electrostatic charge in single-repeat peptides
278 has minimal influence on the peptide assembly on gold. Therefore, further investigation is
279 needed to understand why the outlier exists in our model.

280 4. Discussion

281 When considering the physical implications of the model for f_e in Equation 2, it important to note
282 that the model (linear fit) was not significant when using traditional hydrophobicity scales by
283 Wimley and White [26], or the scale developed by Urry based on elastin [27]. The relationship
284 manifested specifically as a function of relative hydrophobe compatibility with valine. Therefore,
285 we speculate that likely number of hydrophobic interactions, which would be directly related to
286 hydrophobe compatibility with valine (common to all pentapeptide repeats) and the mass loading
287 of the peptides on the surface, is the main predictor of f_e . Similarly, the hydrophobicity of elastin
288 guest residues has been shown to influence mechanical properties [28].

289

290 We also note that secondary structure features of the immobilized ELPs may play a role in the
291 observed model, as they change as a function of hydrophobicity. It has been previously
292 demonstrated that guest residue substitutions, specifically hydrophobicity, can alter the propensity
293 of elastin to form α -, β -, and π -turns in solution [29]. In a recent study, β -turn propensity alone was
294 not a significant driver of ELP properties in solution, but when dimerization was considered, the
295 β -turn content altered ELP properties, specifically hydrophobic accessible surface area [30]. The
296 short ELP surface-assembled structures were investigated in our previous work, where Au-binding
297 was shown to only occur when the cysteine moiety was included in the sequence, and the
298 characteristic β -turn structure was observed when the peptides were immobilized to gold.[16,17,31]
299 In this current study, surface-immobilized triple-repeat ELPs, VKV and KVK, were investigated
300 by atomic force microscopy (AFM), and results are provided in SI (Figure S11). The AFM reveals
301 that the triple-repeat ELPs have distinct topological features when attached to a gold surface.
302 Circular dichroism (CD) was utilized in our study to qualitatively analyze the characteristic
303 features of triple-repeat ELPs in aqueous condition. The secondary structures were more distinct
304 with the increasing fraction of valine (Figure S12), indicating the ELP structures in solution are at
305 least correlated with the results in Figure 3, and surface-bound structure is worthy of future
306 investigation.

307 The importance of the developed model is that it can be used to predict the effective
308 coverage of different short ELPs when immobilized on surfaces with various combinations
309 of guest residues. We note that while it is somewhat analogous to previous models which
310 predict the transition temperature of higher molecular weight ELPs in solution [7,32], our

311 model is not describing LCST behavior, but instead the properties which impact the
312 accessibility of the surface to aqueous components. For example, this model can be applied
313 to designing peptide-functionalized surfaces to control electrode organization, where
314 accessibility of the modified electrode surface is desired. We recently published studies
315 where a single-repeat ELP sequence (X=E) enhanced the ionic transport of a thin ionomer
316 layer, despite being adsorbed to the gold electrodes [15]. This current study shows that a
317 single-repeat peptide where X=E would have relatively low f_e , thus corroborating the results
318 of our previous study. Another area where the model will have impact is in the field of
319 sensor design where ELPs are proposed as an active transducer [11]. It would be ideal to
320 have the greatest difference in f_e between ELP in the soluble and insoluble states, and this
321 study provides a basis on which future work optimizing ELP-based sensor sequences can
322 be built. This study also provides direction for future studies where the impact of bound
323 ELP on redox probe diffusion, electrochemically active surface area, and electron transfer
324 rate will be fully elucidated and quantified.

325 **5. Conclusion**

326 This work elucidates the relationship between effective surface coverage, ELP guest
327 residue, and mass loading for ELP sequences immobilized to gold. Specifically, there exists
328 a linear relationship between effective coverage and the product of the ELP guest residue
329 hydrophobe compatibility with valine and mass loading. This model demonstrates the
330 potential for ELPs to be precisely designed for future electrochemical and biomaterial
331 applications.

332

333 **Associated Content**

334 Supplementary data includes supporting experimental details as well as Figures S1–S12 and
335 Tables S1–S7.

336

337 **Author Contributions**

338 Zihang Su: Conceptualization, methodology, formal analysis, investigation, resources, data
339 curation, writing - original draft, visualization. ChulOong Kim: investigation, formal analysis,
340 writing – review & editing. Julie N. Renner: Conceptualization, methodology, formal analysis,
341 writing – review & editing, supervision, project administration, funding acquisition.

342

343 **Acknowledgements**

344 This work was supported by the United States Department of Agriculture (2018-68011-
345 28691) and the National Science Foundation (1739473). The authors acknowledge Dr.
346 Smarajit Bandyopadhyay for CD assistance, Prof. Chung-Chiun Liu and Dr. Yifan Dai
347 from electronics design center in CWRU for helpful discussions.

348

349

350

351 **References:**

- 352 [1] J.N. Renner, S.D. Minter, Minireview The use of engineered protein materials in
353 electrochemical devices, (2016) 980–985. <https://doi.org/10.1177/1535370216647127>.
- 354 [2] Q. Liu, J. Wang, B.J. Boyd, Peptide-based biosensors, *Talanta*. 136 (2015) 114–127.
355 <https://doi.org/10.1016/j.talanta.2014.12.020>.
- 356 [3] M. Rasmussen, S.D. Minter, *Biosensors and Bioelectronics* Enzymatic biofuel cells : 30
357 years of critical advancements, 76 (2016) 91–102.
358 <https://doi.org/10.1016/j.bios.2015.06.029>.
- 359 [4] D.W. Urry, *Physical Chemistry of Biological Free Energy Transduction As Demonstrated*
360 *by Elastic*, 5647 (1997) 11007–11028. <https://doi.org/10.1021/jp972167t>.
- 361 [5] D.E. Meyer, A. Chilkoti, D.W. Urry, Q. Liu, J. Wang, B.J. Boyd, J.A. MacKay, D.J.
362 Callahan, K.N. FitzGerald, A. Chilkoti, J. Reguera, D.W. Urry, T.M. Parker, D.T.
363 McPherson, J.C. Rodríguez-Cabello, C. Luan, T.M. Parker, D.C. Gowda, K.U. Prasad, M.C.
364 Reid, Quantitative model of the phase behavior of recombinant pH-responsive elastin-like
365 polypeptides, *Biomacromolecules*. 11 (2010) 2873–2879.
366 <https://doi.org/10.1021/bm100571j>.
- 367 [6] J. Reguera, D.W. Urry, T.M. Parker, D.T. McPherson, J.C. Rodríguez-Cabello, Effect of
368 NaCl on the exothermic and endothermic components of the inverse temperature transition
369 of a model elastin-like polymer, *Biomacromolecules*. 8 (2007) 354–358.
370 <https://doi.org/10.1021/bm060936l>.
- 371 [7] D.E. Meyer, A. Chilkoti, Quantification of the effects of chain length and concentration on
372 the thermal behavior of elastin-like polypeptides, *Biomacromolecules*. 5 (2004) 846–851.
373 <https://doi.org/10.1021/bm034215n>.

- 374 [8] D.W. Urry, C.H. Luan, T.M. Parker, D.C. Gowda, K.U. Prasad, M.C. Reid, A. Safavy,
375 Temperature of Polypeptide Inverse Temperature Transition Depends on Mean Residue
376 Hydrophobicity, *J. Am. Chem. Soc.* 113 (1991) 4346–4348.
377 <https://doi.org/10.1021/ja00011a057>.
- 378 [9] A.K. Varanko, J.C. Su, A. Chilkoti, Elastin-Like Polypeptides for Biomedical Applications.,
379 *Annu. Rev. Biomed. Eng.* (2020) 343–369. [https://doi.org/10.1146/annurev-bioeng-](https://doi.org/10.1146/annurev-bioeng-092419-061127)
380 [092419-061127](https://doi.org/10.1146/annurev-bioeng-092419-061127).
- 381 [10] N. Nath, A. Chilkoti, Creating “smart” surfaces using stimuli responsive polymers, *Adv.*
382 *Mater.* 14 (2002) 1243–1247. [https://doi.org/10.1002/1521-](https://doi.org/10.1002/1521-4095(20020903)14:17<1243::AID-ADMA1243>3.0.CO;2-M)
383 [4095\(20020903\)14:17<1243::AID-ADMA1243>3.0.CO;2-M](https://doi.org/10.1002/1521-4095(20020903)14:17<1243::AID-ADMA1243>3.0.CO;2-M).
- 384 [11] M.A. Morales, W.A. Paiva, L. Marvin, E.R.M. Balog, J.M. Halpern, Electrochemical
385 characterization of the stimuli-response of surface-immobilized elastin-like polymers, *Soft*
386 *Matter.* 15 (2019) 9640–9646. <https://doi.org/10.1039/c9sm01681c>.
- 387 [12] C.J. Barile, E.C.M. Tse, Y. Li, T.B. Sobyra, S.C. Zimmerman, A. Hosseini, A.A. Gewirth,
388 Proton switch for modulating oxygen reduction by a copper electrocatalyst embedded in a
389 hybrid bilayer membrane, *Nat. Mater.* 13 (2014) 619–623.
390 <https://doi.org/10.1038/nmat3974>.
- 391 [13] J. Bao, C. Hou, D. Huo, Q. Dong, X. Ma, X. Sun, M. Yang, K.H.A. El Galil, W. Chen, Y.
392 Lei, Sensitive and Selective Electrochemical Biosensor Based on ELP-OPH/BSA/TiO₂
393 NFs/AuNPs for Determination of Organophosphate Pesticides with p -Nitrophenyl
394 Substituent , *J. Electrochem. Soc.* 164 (2017) G17–G22.
395 <https://doi.org/10.1149/2.0311702jes>.
- 396 [14] Y. Lu, H. Ang, Q. Yan, E. Fong, Bioinspired Synthesis of Hierarchically Porous

397 MoO₂/Mo₂C Nanocrystal Decorated N-Doped Carbon Foam for Lithium-Oxygen Batteries,
398 Chem. Mater. 28 (2016) 5743–5752. <https://doi.org/10.1021/acs.chemmater.6b01966>.

399 [15] Z. Su, S. Kole, L.C. Harden, V.M. Palakkal, C. Kim, G. Nair, C.G. Arges, J.N. Renner,
400 Peptide-Modified Electrode Surfaces for Promoting Anion Exchange Ionomer Microphase
401 Separation and Ionic Conductivity, ACS Mater. Lett. 1 (2019) 467–475.
402 <https://doi.org/10.1021/acsmaterialslett.9b00173>.

403 [16] Z. Su, N. Pramounmat, S.T. Watson, J.N. Renner, Engineered interaction between short
404 elastin-like peptides and perfluorinated sulfonic-acid ionomer, Soft Matter. 14 (2018) 3528–
405 3535. <https://doi.org/10.1039/c8sm00351c>.

406 [17] N. Pramounmat, C.N. Loney, C. Kim, L. Wiles, K.E. Ayers, A. Kusoglu, J.N. Renner,
407 Controlling the Distribution of Perfluorinated Sulfonic Acid Ionomer with Elastin-like
408 Polypeptide, ACS Appl. Mater. Interfaces. 11 (2019) 43649–43658.
409 <https://doi.org/10.1021/acсами.9b11160>.

410 [18] J.C.M. Van Hest, X. Xu, V. Lemieux, P.H.H.M. Adams, J.C.M. Van Hest, Elastin-based
411 stimuli-responsive gold nanoparticles w, 46 (2010). <https://doi.org/10.1039/b923280j>.

412 [19] H.C. Huang, Y. Yang, A. Nanda, P. Koria, K. Rege, Synergistic administration of
413 photothermal therapy and chemotherapy to cancer cells using polypeptide-based degradable
414 plasmonic matrices, Nanomedicine. 6 (2011) 459–473. <https://doi.org/10.2217/nmm.10.133>.

415 [20] S. Cheemalapati, M. Ladanov, B. Pang, Y. Yuan, P. Koria, Y. Xia, A. Pyayt, Dynamic
416 visualization of photothermal heating by gold nanocages using thermoresponsive elastin
417 like polypeptides, Nanoscale. 8 (2016) 18912–18920. <https://doi.org/10.1039/c6nr04676b>.

418 [21] K. Vogele, J. List, G. Pardatscher, N.B. Holland, F.C. Simmel, T. Pirzer, Self-Assembled
419 Active Plasmonic Waveguide with a Peptide-Based Thermomechanical Switch, ACS Nano.

- 420 10 (2016) 11377–11384. <https://doi.org/10.1021/acsnano.6b06635>.
- 421 [22] S. Chen, L. Li, C. Zhao, J. Zheng, Surface hydration: Principles and applications toward
422 low-fouling/nonfouling biomaterials, *Polymer (Guildf)*. 51 (2010) 5283–5293.
423 <https://doi.org/10.1016/j.polymer.2010.08.022>.
- 424 [23] A.L. Furst, A.C. Hoepker, M.B. Francis, Quantifying Hormone Disruptors with an
425 Engineered Bacterial Biosensor, *ACS Cent. Sci.* 3 (2017) 110–116.
426 <https://doi.org/10.1021/acscentsci.6b00322>.
- 427 [24] J.C. Biro, Theoretical Biology and Medical Amino acid size , charge , hydrophathy indices
428 and matrices for, *12* (2006) 1–12. <https://doi.org/10.1186/1742-4682-3-15>.
- 429 [25] A. Prhashanna, P.A. Taylor, J. Qin, K.L. Kiick, A. Jayaraman, Effect of Peptide Sequence
430 on the LCST-Like Transition of Elastin-Like Peptides and Elastin-Like Peptide – Collagen-
431 Like Peptide Conjugates : Simulations and Experiments, (2019).
432 <https://doi.org/10.1021/acs.biomac.8b01503>.
- 433 [26] W.C. Wimley, S.H. White, At Membrane Interfaces, *Nat. Structural Biol.* 3 (1996) 842–848.
- 434 [27] D.W. Urry, C.-H. Luan, A New Hydrophobicity Scale and Its Relevance to Protein Folding
435 and Interactions at Interfaces, (1995) 92–110. <https://doi.org/10.1021/bk-1995-0602.ch007>.
- 436 [28] S. Hollingshead, J.C. Liu, pH-Sensitive Mechanical Properties of Elastin-Based Hydrogels,
437 *Macromol. Biosci.* 20 (2020) 1–12. <https://doi.org/10.1002/mabi.201900369>.
- 438 [29] A. Prhashanna, P.A. Taylor, J. Qin, K.L. Kiick, A. Jayaraman, Effect of Peptide Sequence
439 on the LCST-Like Transition of Elastin-Like Peptides and Elastin-Like Peptide-Collagen-
440 Like Peptide Conjugates: Simulations and Experiments, *Biomacromolecules.* 20 (2019)
441 1178–1189. <https://doi.org/10.1021/acs.biomac.8b01503>.
- 442 [30] Y. Zhang, V. Zai-Rose, C.J. Price, N.A. Ezzell, G.L. Bidwell, J.J. Correia, N.C. Fitzkee,

- 443 Modeling the Early Stages of Phase Separation in Disordered Elastin-like Proteins, *Biophys.*
444 *J.* 114 (2018) 1563–1578. <https://doi.org/10.1016/j.bpj.2018.01.045>.
- 445 [31] Z. Su, S. Kole, V.M. Palakkal, L.C. Harden, C. Kim, Peptide-modified electrode surfaces
446 for promoting anion exchange ionomer microphase separation and ionic conductivity, (n.d.)
447 1–24.
- 448 [32] A. Ghoorchian, N.B. Holland, Molecular architecture influences the thermally induced
449 aggregation behavior of elastin-like polypeptides, *Biomacromolecules.* 12 (2011) 4022–
450 4029. <https://doi.org/10.1021/bm201031m>.
- 451